Contents lists available at ScienceDirect

Colloids and Surfaces B: Biointerfaces

journal homepage: www.elsevier.com

Fluorinated CdSe/ZnS quantum dots: Interactions with cell membrane

Pablo G. Argudo[a], María T. Martín-Romero[a], Luis Camacho[a], Mónica Carril[b, c], Carolina Carrillo-Carrión[d, e, **], Juan J. Giner-Casares[a, *]

[a] Institute of Fine Chemistry and Nanochemistry, Department of Physical Chemistry and Applied Thermodynamics, University of Córdoba, Campus Universitario de Rabanales, Edificio Marie Curie, Córdoba, E-14014, Spain
[b] Biofisika Institute (CSIC, UPV/EHU) and Department of Biochemistry and Molecular Biology, University of the Basque Country UPV/EHU, 48940, Leioa, Spain
[c] Ikerbasque, Basque Foundation for Science, Bilbao, 48011, Spain
[d] CIC biomaGUNE, 20014, San Sebastian, Spain
[e] Center for Research in Biological Chemistry and Molecular Materials (CiQUS), University of Santiago de Compostela, 15782, Santiago de Compostela, Spain

ARTICLE INFO

Keywords:
Fluorination
Langmuir monolayers
Quantum dots
Uptake

ABSTRACT

Fluorescent inorganic quantum dots are highly promising for biomedical applications as sensing and imaging agents. However, the low internalization of the quantum dots, as well as for most of the nanoparticles, by living cells is a critical issue which should be solved for success in translational research. In order to increase the internalization rate of inorganic CdSe/ZnS quantum dots, they were functionalized with a fluorinated organic ligand. The fluorinated quantum dots displayed an enhanced surface activity, leading to a significant cell uptake as demonstrated by *in vitro* experiments with HeLa cells. We combined the experimental and computational results of Langmuir monolayers of the DPPC phospholipid as a model cell membrane with *in vitro* experiments for analyzing the mechanism of internalization of the fluorinated CdSe/ZnS quantum dots. Surface pressure-molecular area isotherms suggested that the physical state of the DPPC molecules was greatly affected by the quantum dots. UV–vis reflection spectroscopy and Brewster Angle Microscopy as *in situ* experimental techniques further confirmed the significant surface concentration of quantum dots. The disruption of the ordering of the DPPC molecules was assessed. Computer simulations offered detailed insights in the interaction between the quantum dots and the phospholipid, pointing to a significant modification of the physical state of the hydrophobic region of the phospholipid molecules. This phenomenon appeared as the most relevant step in the internalization mechanism of the fluorinated quantum dots by cells. Thus, this work sheds light on the role of fluorine on the surface of inorganic nanoparticles for enhancing their cellular uptake

1. Introduction

Colloidal inorganic quantum dots (QDs) are highly valued in optoelectronics, [1] with a growing relevance in the biomedical field as sensing and imaging active agents [2–4]. Yet the inefficient internalization of the QDs by living cells remains as one of the most relevant frontiers for the *in vivo* clinical application. Such low internalization issue entails the need of using high doses of QDs. [5] Therefore, the interaction of the QDs with the cell membrane appears key for understanding and designing efficient QDs for biomedical applications. Fluorination of the capping ligands of QDs appears as an efficient strategy to improve the internalization by exploiting the change in polarity to render a high surface activity. [6]Herein we studied the effect of a fluorinated CdSe/ZnS QD on a model cell membrane and its uptake by living cells in high detail. Enhanced cell uptake of QDs coated with fluorinated ligands with respect to non-fluorinated QDs has been observed. A detailed view of the intermolecular interaction of the fluorinated QDs at the cell membrane is aimed. Experimental data have been obtained, additionally including molecular dynamics simulations for an atomistic description. The surface of the cell membrane is modelled as a Langmuir monolayer of the DPPC phospholipid as main constituent of the eukaryotic membranes. [7] The Langmuir technique allows a fine tuning of the available surface area for the phospholipid molecules at the air/water interface. *In situ* microscopy and UV–vis spectroscopy experi-

* Corresponding author.
** Corresponding author at: Biofisika Institute (CSIC, UPV/EHU) and Department of Biochemistry and Molecular Biology, University of the Basque Country UPV/EHU, 48940, Leioa, Spain
Email addresses: carolina.carrillo@usc.es (C. Carrillo-Carrión); jjginer@uco.es (J.J. Giner-Casares)

https://doi.org/10.1016/j.colsurfb.2018.09.050
Received 25 July 2018; Received in revised form 17 September 2018; Accepted 21 September 2018
Available online xxx
0927-7765/ © 2018.

UNCORRECTED PROOF

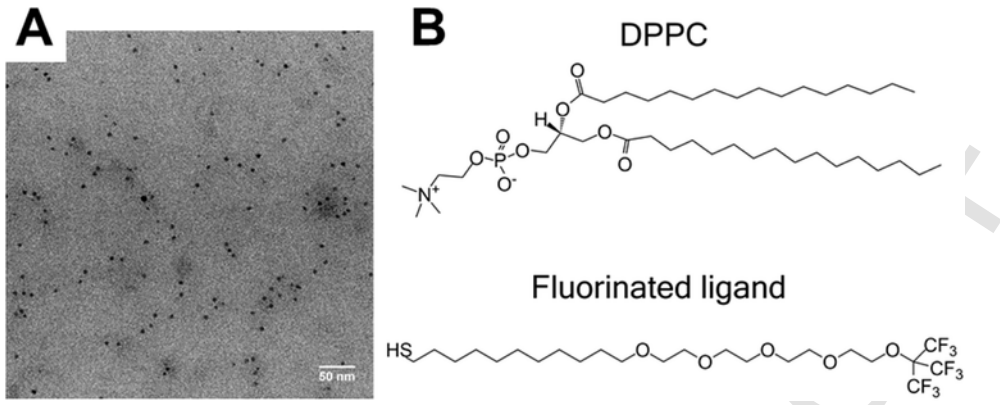

Fig. 1. A) Transmission electron microscopy of fluorinated CdSe/ZnS quantum dots (QD_F). B) Molecular structure of the DPPC phospholipid used herein as model lipid and the fluorinated ligand for capping the CdSe/ZnS quantum dots.

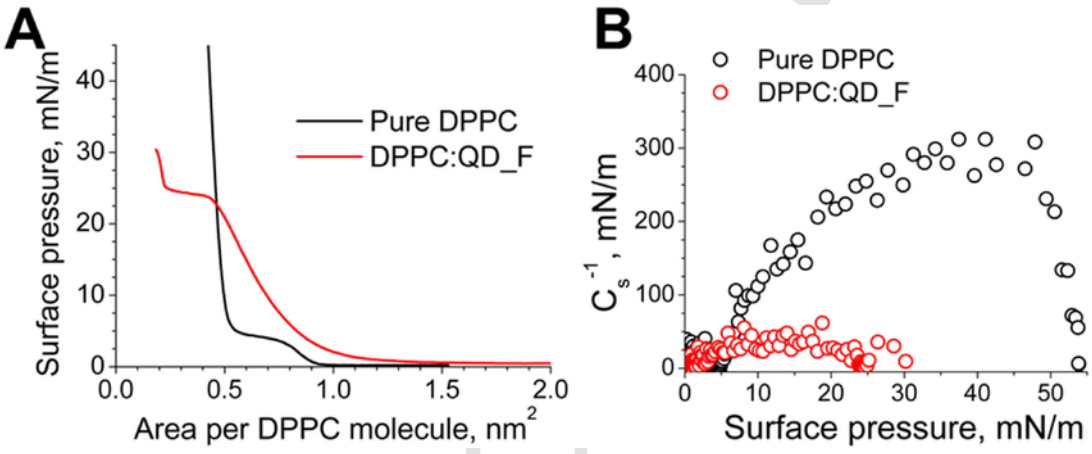

Fig. 2. A) Surface pressure-molecular area isotherms for the DPPC monolayer (black line) and a DPPC monolayer cospread with the QD_F (red line) on pure water as a subphase. B) Compression modulus values *versus* surface pressure for both isotherms, as noted in the inset. (For interpretation of the references to colour in this figure legend, the reader is referred to the web version of this article.)

ments were performed to monitor the effect of the fluorinated QDs on the phospholipid monolayer. [8] Indeed, Langmuir monolayers of phospholipids have been successfully used by the group of Reis et al. to assess the mechanism of action of drugs, quantifying the influence of the drug in the structure on the lipid monolayers, as well as the aggregation state of the drug at the lipid interface [9,10]. Bioactive molecules such as enzymes, have been studied in detail by Caseli et al. at the phospholipid interface using monolayers [11]. Monolayers of inorganic nanoparticles might be also formed at the air/liquid interface, provided the capping ligands display enough hydrophobicity [12,13].

2. Materials and methods

Materials. 1,2-dipalmitoyl-sn-glycero-3-phosphocholine (DPPC, ≥99%) and the chloroform (> 99.9%) were purchased from Aldrich (Germany) and used as received. Chloroform was used as the spreading solvent. The concentration of DPPC in chloroform was 1 mM. The quantum dots (QDs) were included in the spreading solution with DPPC. The molar ratio DPPC:QDs in the spreading solution was 75:1 in all cases. This value of molar ratio ensures that *ca.* 20% of the DPPC molecules are in excess with respect to a complete covering of the DPPC monolayer by an underneath monolayer of quantum dots. Ultrapure water, produced by a Millipore Milli-Q unit, pre-treated by a Millipore reverse osmosis system (>18.2 MΩ cm^{-1}), was used as subphase. The subphase temperature was 21 °C with pH 5.7. Cadmium oxide (CdO, 99.9%) was purchased from Alfa Aesar. Zinc oxide (ZnO, 99.9%), stearic acid (SA, 99%), sulphur powder (S, 99.98%), octadecene (ODE, 90%), hexyldecylamine (HDA, 90%), trioctylphosphine oxide (TOPO, 90%), trioctylphosphine (TOP, 97%), diethylzinc solution ($ZnEt_2$, 1 M in hexane), bis(trimethylsilyl) sulfide ($(TMS)_2S$, 99%), Dimethyl sulfoxide (DMSO), Dichloromethane (DCM) were purchased from Sigma-Aldrich (Germany). All these chemicals were used as received without further purification. All organic solvents used were of analytical grade. The used fluorinated ligand, $HS\text{-}C_{11}\text{-}(EG)_4\text{-}O\text{-}C(CF_3)_3$ (EG = ethyleneglycol), was synthesized as previously reported. [14] Human cervical cancer cell line (HeLa) was purchased from ATCC-LGC. Dulbecco's modified Eagle's medium (DMEM), fetal bovine serum (FBS), and L-glutamine were purchased from Gibco. Penicillin and streptomycin were purchased from Hyclone. The PBS buffer was purchased in tablets and prepared following manufacturer procedures (Sigma-Aldrich) corresponding to 10 mM phosphate buffer containing 137 mM NaCl and 2.7 mM KCl at pH 7.4. Cell Proliferation kit I based on 3(4,5-Dimethylthiazol-2-yl)-2,5-diphenyltetrazolium bromide (MTT assay) was purchased from Roche. 8-well glass Millicell EZ slide was supplied by Millipore and mounting media by Dako.

Fluorination. Fluorinated CdSe/ZnS core-shell quantum dots (in the following referred to as QD_F) were prepared as described previously. [6] Briefly, TOPO-capped CdSe/ZnS QDs (in the following referred to as QD_TOPO) were modified with a fluorinated ligand, $HS\text{-}C_{11}H_{22}\text{-}(EG)_4\text{-}O\text{-}C(CF_3)_3$ (EG = ethyleneglycol) *via* ligand-exchange procedure. The fluorinated ligand and QD_TOPO were reacted in a mixture DCM:MeOH (1:2) and stirred overnight in darkness at 40 °C. 2×10^4 fluorinated ligands per QD were used in order to achieve a complete coverage of the QD surface. Next day, the QD_F nanoparticles

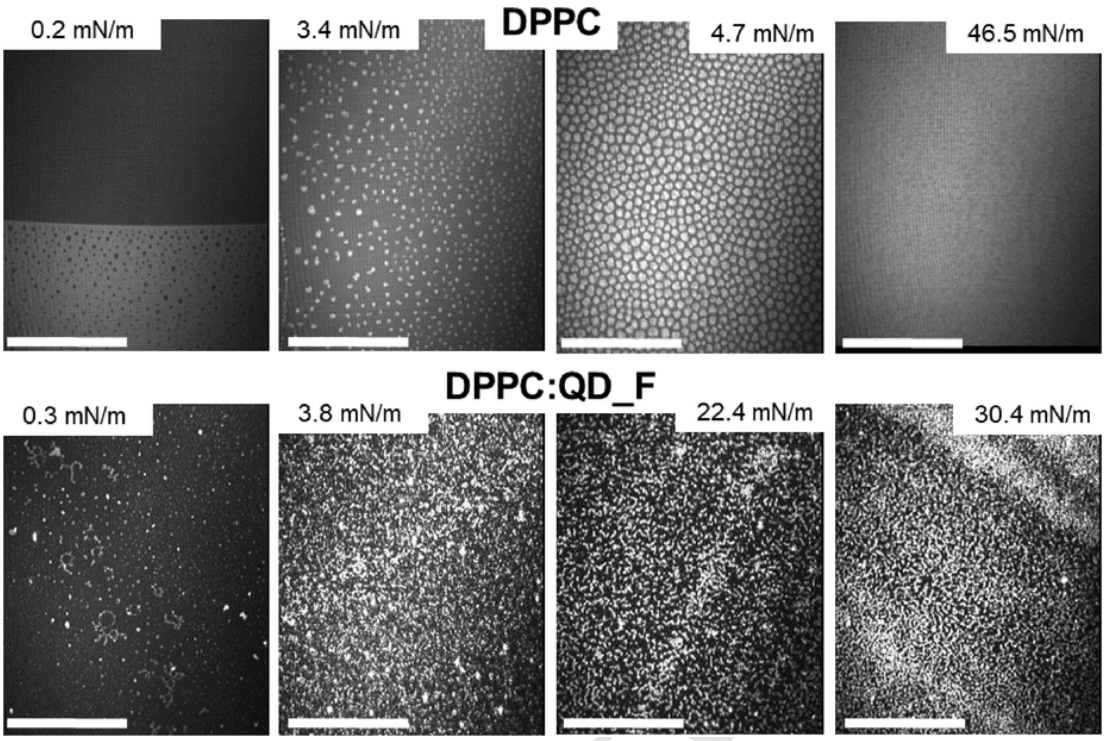

Fig. 3. Brewster Angle Microscopy pictures of the DPPC (top) and a DPPC monolayer cospread with the QD_F (bottom) monolayer on pure water as a subphase. The values of surface pressure for each picture is indicated in the inset. Scale bars equals to 100 μm.

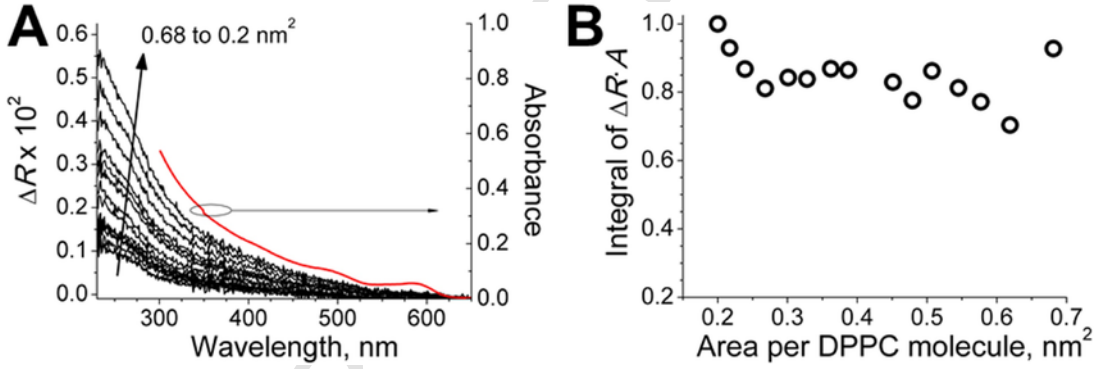

Fig. 4. A) UV–vis reflection spectra of the DPPC monolayer cospread with the QD_F at different values of surface area from 0.7 to 0.2 nm^2 per DPPC molecule, as indicated in the figure (black lines, left axis). UV–vis absorption spectrum of the CdSe/ZnS quantum dots in bulk solution (red line, right axis). B) Values of integrated UV–vis reflection spectra band normalized per surface area as a function of the area per DPPC molecule. (For interpretation of the references to colour in this figure legend, the reader is referred to the web version of this article.)

were purified by centrifugation at 1.5×10^5 RCF for 30 min, and washed three times with MeOH. Finally, the purified QD_F particles were dispersed in DCM and stored in the fridge (4 °C) in darkness until use.

Surface pressure–area isotherms. Two different models of Nima troughs (Nima Technology, Coventry, England) were used in this work, both provided with a Wilhelmy type dynamometric system using a strip of filter paper: a NIMA 611D with one moving barrier for the measurement of the UV–vis reflection spectra, and a NIMA 601, equipped with two symmetrical barriers to record Brewster angle microscopy images. The monolayers were compressed at a speed of 0.03 $nm^2\,min^{-1}$molecule^{-1}.

UV-vis reflection spectroscopy. UV–vis reflection spectra at normal incidence as the difference in reflectivity (ΔR) of the film-covered water surface and the bare surface were obtained with a Nanofilm Surface Analysis Spectrometer (RefSPEC^2, supplied by Accurion GmbH, Göttingen, Germany).

Brewster angle microscopy (BAM). Images of the film morphology were obtained by Brewster angle microscopy with a I-Elli2000 (Accurion GmbH) using a Nd:YAG diode laser with wavelength 532 nm and 50 mW, which can be recorded with a lateral resolution of 2 μm. The image processing procedure included a geometrical correction of the image, as well as a filtering operation to reduce interference fringes and noise.

All instruments for the study of the Langmuir monolayers at the air/liquid interface were located on tables with vibration isolation (antivibration system MOD-2 S, Accurion, Göttingen, Germany) in a large class 100 clean room.

Computer simulations. 36 molecules of the fluorinated ligand were modelled as covalently bound by a S—S bond to the ZnS surface. 0.47 nm^2 was taken as the average value of surface area per fluorinated ligand, corresponding to a dense coating of the QD_F surface. A similar intermolecular distance between the fluorinated ligand molecules was imposed to ensure a homogeneous distribution. The force field Com-

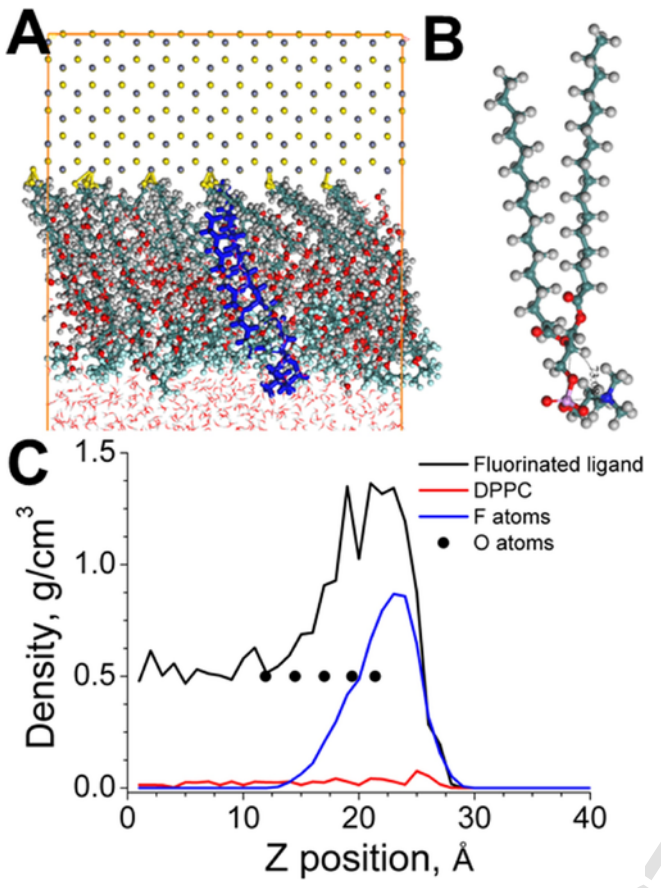

Fig. 5. A) Snapshot of the DPPC molecule in contact with the surface of the QD_F. Top region depicts the inorganic surface. The fluorinated ligands are displayed in green (C atoms), red (O atoms) and light blue (F atoms). The DPPC molecule is highlighted in blue for clarity. Bottom region shows the water molecules. B) Snapshot of the DPPC molecule displaying a tilting angle of the headgroup of 73.1°. C) Distribution of the fluorinated ligand, DPPC, and average position of the oxygen and fluorine atoms along the axis perpendicular to the DPPC monolayer. Zero was placed in the surface of the QD_F. (For interpretation of the references to colour in this figure legend, the reader is referred to the web version of this article.)

passII was used for computation of initial atom charge and optimization of the geometry. Molecular dynamics was applied in the NVE ensemble (T = 298 K, 20 ps of total MD time, time step of 0.1 fs). An additional step of geometry optimization was applied subsequently to the Molecular Dynamics. The XYZ dimension values of the computational box were 45.7 × 37.4 × 137.6 Å^3. The computational results and the molecular arrangement were analysed by in-house software using MathCad 14.0.

Cell viability. Cell viability of HeLa cells after exposure to the QD_F nanoparticles was assessed by using the colorimetric MTT (3-(4,5-dimethylthazolk-2-yl)-2,5-diphenyl tetrazolium bromide) assay. 1 × 10^5 cells were seeded in 96-well plates and cultured for 24 h at 37 °C and 5% CO_2 in complete medium. Then, cells were incubated with either 5 nM of QD_F or 0.5% DMSO (because the QD_F were initially dispersed in DMSO) for 5 h and 24 h in serum-free medium. Untreated cells were used as control. Afterwards, cells were washed twice with 100 μL of serum-free medium and incubated for 30 min at 37 °C and 5% CO_2 with 100 μL of MTT solution (at a dilution 1:20 in medium). The formazan crystals produced by the dehydrogenase mitochondrial activity of living cells were dissolved in 100 μL DMSO, and the absorbance at 550 nm of the MTT product was measured in a microplate reader (Genios Pro, TECAN). Cell viability is expressed as a percentage of absorbance of treated cells related to the untreated control cells and represented as mean of quadruplicates ± standard deviation (SD).

Imaging. Cells were imaged employing a confocal laser scanning microscope (CLSM 510 Meta) from Zeiss, and using a Plan-Apochromat 63x/1.4 M27 oil immersion objective. QD_F internalized by cells were excited with a 405 nm laser diode, and their fluorescence emission was collected in the range 420–500 nm. Transmission images were also collected.

3. Results and discussion

The fluorinated-capped CdSe/ZnS QDs will be referred herein as QD_F. The inorganic core of the QD_F has a diameter of 5.5 ± 0.3 nm as measured for Transmission Electron Microscopy (TEM), see Fig. 1A. The molecular structure of the DPPC phospholipid and the fluorinated capping ligand for the QD_F are shown in Fig. 1B. In contrast to either purely hydrophobic or hydrophilic ligands, this fluorinated capping agent was purposefully designed to provide the QD_F with a significant surface activity, aimed at improving the cell uptake.

The QD_F was studied in a cospread solution with the DPPC molecules to build a Langmuir monolayer with the DPPC molecules in close contact with the QD_F. The impact of the QD_F at the phospholipid interface on the DPPC molecules was significant, see Fig. 2A. A modification of the surface pressure-molecular area isotherm was observed with respect to the isotherm for the pure DPPC monolayer. [15] Two main

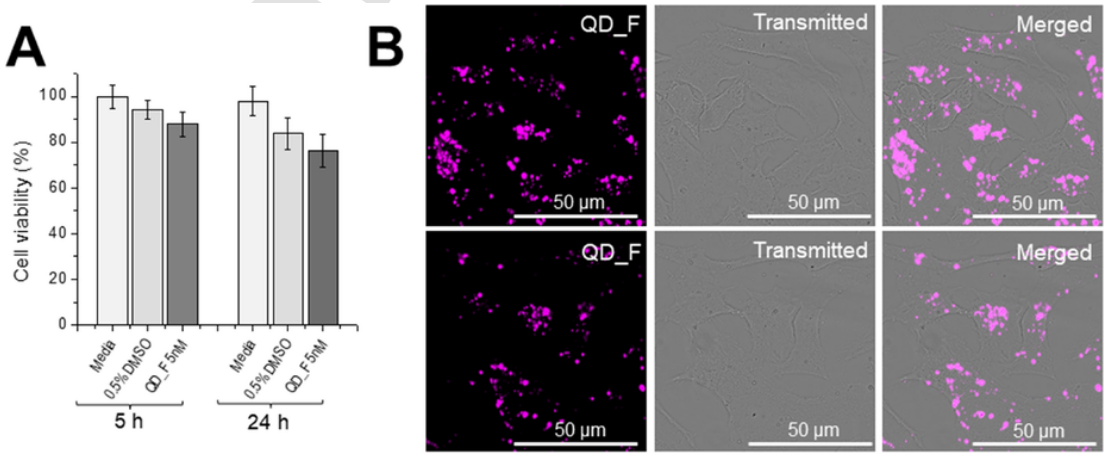

Fig. 6. A) Cell viability obtained by MTT assay of HeLa cells incubated for either 5 h or 24 h with 0.5% DMSO or QD_F at 5 nM. QD_F were dispersed in serum-free cell medium containing 0.5% DMSO. B) Confocal microscopy images of HeLa cells after incubation for 5 h at 37 °C with 5 nM of QD_F NPs. Incubation was performed in serum-free DMEM cell media containing 0.5% of DMSO. Fluorescence channel was collected at 420–500 nm (λ_{exc} 405 nm). Single fluorescence channel and merged with the transmitted light channel are shown.

regions of the DPPC:QD_F isotherm might be defined. Firstly, an expansion of the DPPC:QD_F isotherm with respect to the DPPC could be observed at values of surface pressure lower than *ca.* 23 mN/m. This expansion of the DPPC isotherm in presence of the QD_F indicated the occupancy of the monolayer by the QD_F similarly to organic molecules as thymol. [16] The interaction between the QD_F and the DPPC molecules occurred mainly at the hydrophobic region of the monolayer. This interaction modified the physical state of the alkyl chains of the DPPC phospholipids, see below [17]. The lateral repulsion between adjacent molecules existing in the supramolecular structure might contribute as well to the expansion of the isotherm. An intercrossing of the isotherms took place at *ca.* 23 mN/m. Secondly, a decrease in the molecular area of the DPPC:QD_F isotherm with respect to the DPPC was obtained for values of surface pressure greater than 23 mN/m. This modification of the surface pressure-molecular area isotherm was ascribed to a condensation of the phospholipid monolayer. [18] QD_F could be expelled from the DPPC monolayer upon further compression, sitting on the alkyl chains of the compressed DPPC monolayer. The strong hydrophobicity of the QD_F provoked the removal of DPPC molecules from the air/water interface to the surface of the QD_F. Computer simulations further confirmed the interdigitation of the DPPC molecules and the fluorinated ligand of the QD_F, see below. A reduction of the effective number of DPPC molecules at the air/water interface was then obtained upon the intercrossing of the surface pressure-molecular area isotherms of DPPC and DPPC:QD_F, see Fig. 2. An early collapse was obtained upon further compression of the DPPC monolayer.

Compression modulus is defined as $C_s^{-1} = -(d\pi/dA)_T$, offering a quantitative indication on the physical state of the DPPC monolayer. [19] Liquid-expanded (LE) state of the monolayers is defined for values of compression modulus in the range from 10 to 50 mN/m, obtained for the DPPC monolayer from the offset of the surface pressure up to *ca.* 10 mN/m. A liquid-condensed (LC) state is expected for values of compression modulus between 100 and 250 mN/m, obtained for the DPPC monolayer in the range of values of surface pressure from *ca.* 10 to 25 mN/m. Further compression of the DPPC monolayer resulted in the so-called solid phase, with values greater than 250 mN/m up to the collapse of the DPPC monolayer. Such behavior is expected for a pure DPPC monolayer. [15] The interactions between the QD_F and DPPC molecules were significant, as suggested by the isotherms and confirmed by the compression modulus, see Fig. 2B. A significant fluidization of the DPPC monolayer was obtained in the presence of QD_F. The values of the compression modulus were restricted below 50 mN/m along the complete surface pressure-molecular area isotherm. Therefore the ordering of the alkyl chains of the DPPC was highly disrupted by the presence of the QD_F at the phospholipid interface.

Brewster Angle Microscopy (BAM) allows *in situ* monitoring the formation of different phases and segregation processes at the phospholipid monolayers. [20] The expected domains for the LE/LC phase transition were obtained in the BAM images for the DPPC monolayer, see Fig. 3A. These domains were similar to those previously published in the literature. [21] The morphology of the DPPC monolayer was greatly modified by the presence of the QD_F along the complete surface pressure-molecular area isotherm, see Fig. 3B. Bright and small structures with no defined shape were present already at low values of surface pressure, being assigned to aggregates of QD_F. The surface activity of QD_F led to the presence of the bright aggregates together with the DPPC molecules regardless of the surface pressure value. The high brilliance of the aggregates of the QD_F with the DPPC molecules arised from the absorption at 532 nm and high electronic density of the QD_F, causing the enhanced reflection of incoming radiation at the interface. [22] The mixed structures of DPPC and QD_F were relatively ordered at the interface and do not coalesce upon compression of the monolayer. Thus a restricted attractive interaction between the aggregates of DPPC and QD_F was expected, leading to a disordering effect to the DPPC monolayer [23]. The absence of coalescence of the QD_F aggregates was consistent with the adsorption of DPPC molecules onto the surface of the QD_F. Further aggregation and growth of a solid phase of QD_F was then prevented by the surrounding DPPC molecules.

The morphology observed by BAM was consistent with the thermodynamical insights obtained by the surface pressure-molecular area isotherms and compression modulus, see above. The hydrophobic interactions between the alkyl chains of the DPPC monolayers were not able to maintain the monolayer structure of the pure DPPC when the QD_F were present at the interface, due to the significant interactions with the QD_F. The hydrophobic interactions between the QD_F and the QD_F with the DPPC molecules determined the structuring of the DPPC:QD_F monolayer. [24]

The amount of QD_F present at the phospholipid interface could be quantitatively monitored by *in situ* UV–vis reflection spectroscopy at the air/water interface. [25] The UV–vis band at the air/water interface confirmed the aggregation of the QD_F at the DPPC monolayer when compared to the UV–vis absorption spectrum recorded for a bulk solution of QD_F, see Fig. 4A. The 2D aggregation of the QD_F at the air/water interface caused a shift and broadening of the UV–vis bands. An increase of the intensity in the reflection band with compression of the monolayer was recorded, as expected from the increase on the surface concentration of QD_F. [26]

The normalized UV–vis reflection signal (ΔR_{norm}) to the available surface area per DPPC molecule is defined in eq. (1):

$$\Delta R_{\mathrm{norm}} = A_{DPPC} \times \Delta R = \frac{2.303 \cdot 10^{17} f_0 \varepsilon}{N_{\mathrm{A}}} \sqrt{R_S} \quad (1)$$

where ΔR_{norm} represents the normalized UV–vis reflection signal, obtained as the product of the measured absolute UV–vis reflection signal by the available surface area of the DPPC molecules. ε and f_0 denote the absorption coefficient and an orientation factor accounting for a given preferred orientation of the QD_F, respectively. Note that in this case the $f_0 = 1$, given the spherical shape of the QD_F. The integral value of the normalized UV–vis reflection band could be used to monitor the evolution of the amount of QD_F at the interface with the compression of the DPPC monolayer. This amount of QD_F was expressed relatively to the maximum amount of QD_F at the phospholipid interface, see Fig. 4B. ΔR_{norm} would have a value of unity along the isotherm in case of a constant amount of QD_F at the interface per DPPC molecule, which was not the experimental result. Upon compression of the monolayer, the interaction of the QD_F with the phospholipid molecules was increased, achieving the maximum density of QD_F for a highly compressed DPPC monolayer. The DPPC monolayer in such solid state offered a highly dense surface of hydrophobic chains to interact with the QD_F. Note that at least 80% of the QD_F were present at the phospholipid interface along the complete surface pressure-molecular area, confirming a significant surface activity of the QD_F. The remaining fraction of added QD_F were assumed to be present in the subphase as assemblies. [6] Two minima in the ΔR_{norm} values were observed at *ca.* 0.48 and 0.27 nm^2 per DPPC molecule. These ΔR_{norm} minima appeared at the initial and final points of almost constant surface pressure with reduction of the molecular area in the DPPC:QD_F isotherm, see above. Thus, a rearrangement of the DPPC molecules in this region was expected, probably corresponding to the mentioned adsorption of DPPC molecules onto the QD_F. Note that with the compression of the DPPC monolayer, QD_F diffused towards the monolayer, effectively interacting with the DPPC molecules. Due to the fluidization of the DPPC monolayer provoked by the QD_F, the maximum surface density of QD_F was achieved for values of surface pressure close to 30 mN/m, taken as the equivalent pressure for a monolayer to

UNCORRECTED PROOF

a biological membrane. [27,28] The QD_F were therefore able to effectively exert a significant fluidization of the DPPC monolayer. The maximum surface density of QD_F in contact with the DPPC monolayer was achieved for values of surface pressure close to 30 mN/m as suggested by the BAM pictures and further confirmed by the UV–vis reflection spectra.

Molecular dynamics simulations were performed to attain atomistic insights into the interaction of the fluorinated ligand of the QD_F with the DPPC phospholipid molecules. [29] The computational box is shown in Fig. 5A, displaying the fluorinated ligand molecules in contact with a DPPC molecule. Surprisingly, the interaction of the fluorinated ligands with the hydrophobic tails of the DPPC molecules resulted in the inclusion of the alkyl chains into the layer of the fluorinated ligand. The polar headgroup of the DPPC molecule remained in contact with the water layer. The tilting angle of the polar headgroup is the vector defined by the P—N atoms with respect to the alkyl chains, reaching a value of 73.1°, see Fig. 3B. A significant modification with respect to the expected value of *ca.* 90° was therefore found. [30] The distribution of the fluorine atoms along the Z axis showed a maximum peak toward the outer region of the coating ligands as expected, see Fig. 5C. The average position of the O atoms of the fluorinated ligand showed an almost constant interatomic distance. Remarkably, a significant hydration of the O atoms of the fluorinated ligand was found. The number of H-bonds formed by the O atoms and water molecules from the inner to outer O atoms were 2.2, 1.8, 1.9, 1.4 and 0.4, respectively. The relatively hydrophilic region formed by the hydrated atoms O of the fluorinated ligand was able to accommodate the polar layer of the DPPC molecule including the carbonyl and ester oxygen. The repulsion of the polar headgroup of the DPPC molecule and the F atoms of the capping ligand led to the observed modification of the P—N tilting angle, as commented above. The sum of hydrophobic and polar interactions between the fluorinated ligand and the DPPC molecules resulted in the experimentally observed modification of the DPPC monolayer by the QD_F. The inclusion of the DPPC molecules onto the coating layer of the QD_F could result in the effective removal of DPPC molecules from the monolayer for a compression of the monolayer beyond surface pressure values of *ca.* 23 mN/m, as indicated by the surface pressure-molecular area isotherms.

In vitro cell uptake and imaging experiments were conducted to obtain insights on the interaction of the QD_F with living cells, using HeLa cells as model cell line. [31] The cell viability was decreased to *ca.* 85% after 5 h of incubation with QD_F. A further decrease to *ca.* 75% was obtained after 24 h of incubation, see Fig. 6. DMSO was required to disperse QD_F and perform the cell studies. The contribution by the DMSO solvent to the reduction in cell viability was rather low. Incubation time for imaging experiments was 5 h, rendering a significant uptake of QD_F by the HeLa cells. Confocal fluorescence microscopy showed a significant uptake of QD_F by the HeLa cells, see Fig. 6 [32].

4. Conclusions

The interaction of the fluorinated CdSe/ZnS quantum dot (QD_F) with model cell membranes has been characterized in large detail by using a model DPPC phospholipid Langmuir monolayer. The surface pressure-molecular area isotherms point to a fluidization of the DPPC molecules induced by the presence and effective interaction of the QD_F at the DPPC phospholipid monolayer. *In situ* UV–vis reflection spectroscopy and Brewster Angle Microscopy could confirm the occupancy of the DPPC monolayer by the QD_F and the removal of DPPC molecules to the surface of the QD_F. Molecular dynamics simulations have demonstrated the inclusion of the alkyl chains of the DPPC in the defects of the capped surface of the QD_F. *In vitro* experiments with living cells showed excellent uptake of the QD_F. As a result of the fluidization of the alkyl chains due to the significant interaction of the QD_F with the phospholipid molecules, the mechanism of uptake is proposed as passage of the QD_F through the membrane promoted by hydrophobic interactions. This work suggests that fluorination of the capping ligands of inorganic quantum dots may be a suitable and universal route for enhancing their cell uptake, potentially increasing the biological and clinical application of inorganic quantum dots.

Author contributions

The manuscript was written through contributions of all authors. All authors have given approval to the final version of the manuscript.

Acknowledgment

Support from the Ministry of Economy and Competitiveness of Spain is acknowledged through the CTQ2017-83961-R project. J.J.G.-C. acknowledges the Ministry of Economy and Competitiveness of Spain for a Ramon y Cajal contract (#RyC-2014-14956). C. C.-C. acknowledges the Ministry of Economy and Competitiveness of Spain for a Juan de la Cierva–Incorporación contract (IJCI-2014-19614).

References

[1] M. Liu, O. Voznyy, R. Sabatini, F.P. García de Arquer, R. Munir, A.H. Balawi, X. Lan, F. Fan, G. Walters, A.R. Kirmani, S. Hoogland, F. Laquai, A. Amassian, E.H. Sargent, Hybrid organic–inorganic inks flatten the energy landscape in colloidal quantum dot solids, Nat. Mater. 16 (2017) 258–263, https://doi.org/10.1038/nmat4800.

[2] J. Owen, L. Brus, Chemical synthesis and luminescence applications of colloidal semiconductor quantum dots, J. Am. Chem. Soc. 139 (2017) 10939–10943, https://doi.org/10.1021/jacs.7b05267.

[3] B. Yang, B. Chen, M. He, B. Hu, Quantum dots labeling strategy for "Counting and Visualization" of HepG2 cells, Anal. Chem. 89 (2017) 1879–1886, https://doi.org/10.1021/acs.analchem.6b04314.

[4] H.Y. Yang, Y. Fu, M.-S. Jang, Y. Li, W.P. Yin, T.K. Ahn, J.H. Lee, H. Chae, D.S. Lee, CdSe@ZnS/ZnS quantum dots loaded in polymeric micelles as a pH-triggerable targeting fluorescence imaging probe for detecting cerebral ischemic area, Colloids Surf., B 155 (2017) 497–506, https://doi.org/10.1016/j.colsurfb.2017.04.054.

[5] J.J. Giner-Casares, M. Henriksen-Lacey, M. Coronado-Puchau, L.M. Liz-Marzán, Inorganic nanoparticles for biomedicine: where materials scientists meet medical research, Mater. Today 19 (2016) 19–28, https://doi.org/10.1016/j.mattod.2015.07.004.

[6] C. Carrillo-Carrión, M. Atabakhshi-Kashi, M.M. Carril, K. Khajeh, W.J. Parak, Taking advantage of hydrophobic fluorine interactions for self-assembled quantum dots as a delivery platform for enzymes, Angew. Chem. Int. Ed. 57 (2018) 5033–5036, https://doi.org/10.1002/anie.201801155.

[7] K.D. de Souza, K.R. Perez, N. Durán, G.Z. Justo, L. Caseli, Interaction of violacein in models for cellular membranes: regulation of the interaction by the lipid composition at the air-water interface,, Colloids Surf., B 160 (2017) 247–253, https://doi.org/10.1016/j.colsurfb.2017.09.027.

[8] J.J. Giner-Casares, G. Brezesinski, H. Möhwald, Langmuir monolayers as unique physical models, Curr. Opin. Colloid Interface Sci. 19 (2014) 176–182, https://doi.org/10.1016/j.cocis.2013.07.006.

[9] A.C. Alves, C. Nunes, J. Lima, S. Reis, Daunorubicin and doxorubicin molecular interplay with 2D membrane models,, Colloids Surf., B 160 (2017) 610–618, https://doi.org/10.1016/j.colsurfb.2017.09.058.

[10] D. Lopes, C. Nunes, P. Fontaine, B. Sarmento, S. Reis, Proof of pore formation and biophysical perturbations through a 2D amoxicillin-lipid membrane interaction approach, Biochim. Biophys. Acta - Biomembr. 1859 (2017) 803–812, https://doi.org/10.1016/j.bbamem.2017.01.031.

[11] Fábio de Paula Ayoub, L. Caseli, Controlling the molecular architecture of lactase immobilized in Langmuir-Blodgett films of phospholipids to modulate the enzyme activity,, Colloids Surf., B 150 (2017) 8–14, https://doi.org/10.1016/j.colsurfb.2016.11.015.

[12] S.M. Bradford, E.A. Fisher, M.-V. Meli, Ligand shell composition-dependent effects on the apparent hydrophobicity and film behavior of gold nanoparticles at the air–water interface, Langmuir 32 (2016) 9790–9796, https://doi.org/10.1021/acs.langmuir.6b02238.

[13] A. Raveendran, C. DeWolf, W. Bu, S. McWhirter, M. Meron, B. Lin, M.-V. Meli, Langmuir Films of n-alkanethiol-capped gold nanoparticles and n-alkanes: interfacial mixing scenarios assessed by X-ray reflectivity and grazing incidence diffraction, J. Phys. Chem. C122 (2018) 2975–2982, https://doi.org/10.1021/acs.jpcc.7b09874.

[14] O. Michelena, D. Padro, C. Carrillo-Carrión, P. del Pino, J. Blanco, B. Arnaiz, W.J. Parak, M. Carril, Novel fluorinated ligands for gold nanoparticle labelling with ap-

UNCORRECTED PROOF

plications in 19 F-MRI, Chem. Commun. 53 (2017) 2447–2450, https://doi.org/10.1039/C6CC08900C.
[15] A. Aroti, E. Leontidis, E. Maltseva, G. Brezesinski, Effects of Hofmeister anions on DPPC Langmuir monolayers at the air−water interface, J. Phys. Chem. B 108 (2004) 15238–15245, https://doi.org/10.1021/jp0481512.
[16] J.V.N. Ferreira, T.M. Capello, L.J.A. Siqueira, J.H.G. Lago, L. Caseli, Mechanism of action of Thymol on cell membranes investigated through lipid Langmuir monolayers at the air–water interface and molecular simulation, Langmuir 32 (2016) 3234–3241, https://doi.org/10.1021/acs.langmuir.6b00600.
[17] C. Pereira-Leite, C. Nunes, J.C. Bozelli, S. Schreier, C.S. Kamma-Lorger, I.M. Cuccovia, S. Reis, Can NO-indomethacin counteract the topical gastric toxicity induced by indomethacin interactions with phospholipid bilayers,, Colloids Surf., B 169 (2018) 375–383, https://doi.org/10.1016/j.colsurfb.2018.05.019.
[18] T.E. Goto, C.C. Lopes, H.B. Nader, A.C.A. Silva, N.O. Dantas, J.R. Siqueira, L. Caseli, CdSe magic-sized quantum dots incorporated in biomembrane models at the air–water interface composed of components of tumorigenic and non-tumorigenic cells, Biochim. Biophys. Acta - Biomembr. 1858 (2016) 1533–1540, https://doi.org/10.1016/j.bbamem.2016.04.009.
[19] J.L. Fidalgo Rodríguez, P. Dynarowicz-Latka, J. Miñones Conde, Structure of unsaturated fatty acids in 2D system, Colloids Surf., B 158 (2017) 634–642, https://doi.org/10.1016/j.colsurfb.2017.07.016.
[20] M. Mottola, R.V. Vico, M.E. Villanueva, M.L. Fanani, Alkyl esters of L-ascorbic acid: stability, surface behaviour and interaction with phospholipid monolayers, J. Colloid Interface Sci. 457 (2015) 232–242, https://doi.org/10.1016/j.jcis.2015.07.014.
[21] D.S. Alvares, M.L. Fanani, J. Ruggiero Neto, N. Wilke, The interfacial properties of the peptide Polybia-MP1 and its interaction with DPPC are modulated by lateral electrostatic attractions, Biochim. Biophys. Acta - Biomembr. 1858 (2016) 393–402, https://doi.org/10.1016/j.bbamem.2015.12.010.
[22] C. Roldán-Carmona, J.J. Giner-Casares, M. Pérez-Morales, M.T. Martín-Romero, L. Camacho, Revisiting the Brewster angle microscopy: the relevance of the polar headgroup, Adv. Colloid Interface Sci. 173 (2012) 12–22.
[23] M. Orczyk, K. Wojciechowski, G. Brezesinski, Disordering effects of Digitonin on phospholipid monolayers, Langmuir 33 (2017) 3871–3881, https://doi.org/10.1021/acs.langmuir.6b04613.
[24] A. Wnętrzak, K. Makyła-Juzak, A. Chachaj-Brekiesz, E. Lipiec, N.V. Romeu, P. Dynarowicz-Latka, Cyclosporin A distribution in cholesterol-sphingomyelin artificial membranes modeled as Langmuir monolayers,, Colloids Surf., B 166 (2018) 286–294, https://doi.org/10.1016/j.colsurfb.2018.03.031.
[25] C. Rubia-Payá, G. De Miguel, M.T. Martín-Romero, J.J. Giner-Casares, L. Camacho, UV-Vis Reflection-Absorption Spectroscopy at air-liquid interfaces, Adv. Colloid Interface Sci. 225 (2015) https://doi.org/10.1016/j.cis.2015.08.012.
[26] J.P. Coelho, M.J. Mayoral, L. Camacho, M.T. Martín-Romero, G. Tardajos, I. López-Montero, E. Sanz, D. Ávila-Brande, J.J. Giner-Casares, G. Fernández, A. Guerrero-Martínez, Mechanosensitive gold colloidal membranes mediated by supramolecular interfacial self-assembly, J. Am. Chem. Soc. 139 (2017) 1120–1128, https://doi.org/10.102l/jacs.6b09485.
[27] F. Bringezu, M. Majerowicz, E. Maltseva, S. Wen, G. Brezesinski, A.J. Waring, Penetration of the antimicrobial peptide Dicynthaurin into phospholipid monolayers at the liquid–air interface, ChemBioChem 8 (2007) 1038–1047, https://doi.org/10.1002/cbic.200600503.
[28] O.G. Travkova, H. Moehwald, G. Brezesinski, The interaction of antimicrobial peptides with membranes, Adv. Colloid Interface Sci. 247 (2017) 521–532, https://doi.org/10.1016/j.cis.2017.06.001.
[29] Z. Zheng, J. Saar, B. Zhi, T.A. Qiu, M.J. Gallagher, D.H. Fairbrother, C.L. Haynes, K. Lienkamp, Z. Rosenzweig, Structure–property relationships of amine-rich and membrane-disruptive Poly(oxonorbornene)-coated gold nanoparticles, Langmuir 34 (2018) 4614–4625, https://doi.org/10.1021/acs.langmuir.7b04285.
[30] E.N. Frigini, J.J. López Cascales, R.D. Porasso, Molecular dynamics simulations of Glyphosate in a DPPC lipid bilayer, Chem. Phys. Lipids213 (2018) 111–117, https://doi.org/10.1016/j.chemphyslip.2018.04.003.
[31] Z. Liu, X. Zhou, Y. Miao, Y. Hu, N. Kwon, X. Wu, J. Yoon, A Reversible fluorescent probe for real-time quantitative monitoring of cellular Glutathione, Angew. Chem. Int. Ed. 56 (2017) 5812–5816, https://doi.org/10.1002/anie.201702114.
[32] R.L. Arrowsmith, P.A. Waghorn, M.W. Jones, A. Bauman, S.K. Brayshaw, Z. Hu, G. Kociok-Köhn, T.L. Mindt, R.M. Tyrrell, S.W. Botchway, J.R. Dilworth, S.I. Pascu, Fluorescent gallium and indium bis(thiosemicarbazonates) and their radiolabelled analogues: Synthesis, structures and cellular confocal fluorescence imaging investigations, Dalton Trans. 40 (2011) 6238, https://doi.org/10.1039/c1dt10126a.

UNCORRECTED PROOF